Phase transitions and thermal expansion in pyroelectric energy conversion

Ian M. McKinley and Laurent Pilon[a)]
Mechanical and Aerospace Engineering Department, Henry Samueli School of Engineering and Applied Science, University of California-Los Angeles, 420 Westwood Plaza, Los Angeles, California 90095, USA

(Received 1 November 2012; accepted 29 December 2012; published online 18 January 2013)

This paper elucidates dynamic effects of phase transitions and thermal expansion on pyroelectric energy conversion. The Olsen cycle was performed on [001]-oriented $0.72PbMg_{1/3}Nb_{2/3}O_3$-$0.28PbTiO_3$ (PMN-28PT) single crystals at different frequencies with electric field cycled between 0.2 and 0.75 MV/m and temperature between 22 and 140 °C. The measured energy density more than doubled as frequency increased from 0.0173 to 0.0211 Hz. This was attributed to secondary pyroelectric effect caused by thermal expansion. At 0.0211 Hz, the samples transitioned from pseudocubic to highly polarized tetragonal phase during cooling. At lower frequency, it underwent additional phase transition from tetragonal to less polarized monoclinic phase. © *2013 American Institute of Physics*. [http://dx.doi.org/10.1063/1.4776668]

The rising awareness and research in sustainable and efficient energy technologies has stimulated efforts in harvesting thermal energy that would otherwise be wasted. The Olsen cycle[1] performed on pyroelectric materials relies on time-dependent temperature oscillations to convert thermal energy directly into electricity. Pyroelectric materials possess a temperature-dependent spontaneous polarization defined as the average electric dipole moment per unit volume in the absence of an applied electric field.[2] Fig. 1 shows the isothermal bipolar hysteresis curves (D-E loops) between the electric displacement D and electric field E exhibited by a typical pyroelectric material at two different temperatures T_{cold} and T_{hot}. These so-called D-E loops traveled in the counter-clockwise direction. The electric displacement D of a pyroelectric material at temperature T under high electric field E can be expressed as[3,4]

$$D(E,T) = \epsilon_0\epsilon_r(T)E + P_s(T), \tag{1}$$

where ϵ_o is the vacuum permittivity ($=8.854 \times 10^{12}$ F/m) and $\epsilon_r(T)$ is the large-field dielectric constant. The saturation polarization $P_s(T)$ is equal to the electric displacement extrapolated to zero electric field in the linear region of D vs. E observed under high field[5] and the slope of this linear fit corresponds to the product $\epsilon_0\epsilon_r(T)$. The remnant polarization P_r is another important property defined as the polarization of the material upon removal of the electric field. The Curie temperature T_{Curie} is defined as the temperature at which a ferroelectric material undergoes a phase transition from ferroelectric to paraelectric and corresponds to a maximum in the real part of the complex dielectric constant.[6]

The Olsen cycle consists of two isothermal and two isoelectric field processes in the D-E diagram.[1] The first process of the Olsen cycle corresponds to an increase in electric field from E_L to E_H at constant temperature T_{cold}. The second process consists of heating the material from T_{cold} to T_{hot} under constant electric field E_H. The third process corresponds to a decrease in the electric field from E_H to E_L at constant temperature T_{hot}. Finally, the cycle is closed by cooling the material from T_{hot} to T_{cold} under constant electric field E_L. The generated energy density N_D is defined as the electrical energy produced per unit volume of the material per cycle (in J/l/cycle). It is defined as[1]

$$N_D = \oint E\mathrm{d}D. \tag{2}$$

The power density P_D is the amount of energy generated by the pyroelectric material per unit volume per unit time. It is expressed in W/l and defined as $P_D = N_D f$, where f is the overall cycle frequency defined as $f = (\tau_{12} + \tau_{23} + \tau_{34} + \tau_{41})^{-1}$, where τ_{ij} is the duration of process i-j.

Kandilian *et al.*[7] derived a model estimating the energy density generated by relaxor ferroelectrics undergoing the Olsen cycle given by

$$N_D = (E_H - E_L)\left[\frac{\epsilon_0}{2}[\epsilon_r(T_C) - \epsilon_r(T_H)](E_H + E_L)\right] + (E_H - E_L)\left[P_s(T_C) - P_s(T_H) + \frac{d_{33}x_3}{s_{33}}\right], \tag{3}$$

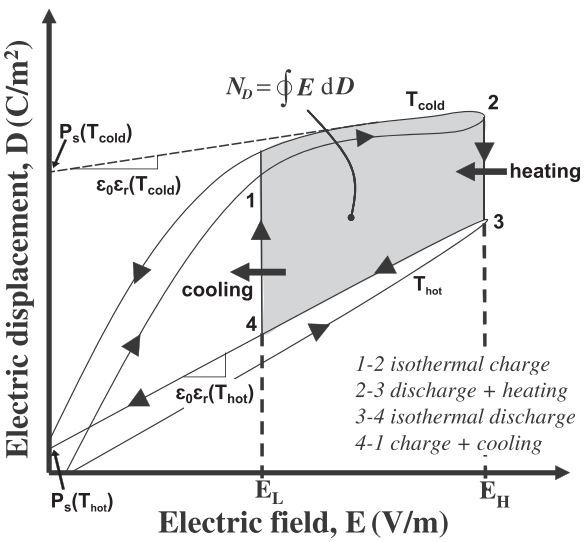

FIG. 1. D-E loops for a typical pyroelectric material at temperatures T_{hot} and T_{cold} and the Olsen cycle performed under quasiequilibrium conditions. N_D is represented by the gray area enclosed by 1-4.

[a)]Author to whom correspondence should be addressed. Electronic mail: pilon@seas.ucla.edu.

where $\epsilon_r(T_C)$ and $\epsilon_r(T_H)$ are the low-frequency ($\sim$0.1 Hz) large-field dielectric constants of the pyroelectric material at the cold and hot source temperatures T_C and T_H, respectively. The last term on the right-hand side of Eq. (3) represents the contribution of the secondary pyroelectric coefficient to the generated energy density due to dimensional changes in the crystal structure caused by temperature changes. Here, d_{33} is the piezoelectric coefficient of the single crystal (in C/N) and s_{33} its elastic compliance (in m^2/N). The strain resulting from temperature change from T_C to T is defined as $x_3 = \int_{T_C}^{T} \alpha_3(T)\,dT$, where $\alpha_3(T)$ is the thermal expansion coefficient (in K^{-1}). This model was validated against experimental data collected on $0.68PbMg_{1/3}Nb_{2/3}O_3$-$0.32PbTiO_3$ (PMN-32PT) single crystal samples[7] using $\epsilon_r(T)$ and $P_s(T)$ reported in the literature.[5] The authors observed that the Olsen cycle exceeded the bounds of the isothermal D-E loops at the silicone oil bath temperatures T_C and T_H. They attributed this to the secondary pyroelectric effect occurring during the heating process 3-4 featuring a rhombohedral to tetragonal phase transition. Equation (3) was also validated with $0.945PbZn_{1/3}$ $Nb_{2/3}O_3$-$0.055PbTiO_3$ (PZN-5.5PT) single crystal samples[8] and with lanthanum-doped zirconate titanate (8/65/35 PLZT) ceramics.[9] But then, the thermal expansion term was ignored because the Olsen cycle fell within the bounds of the isothermal D-E loops at T_C and T_H. The goal of this model was to rapidly characterize the energy density of materials undergoing the Olsen cycle without physically having to perform the cycle. However, without performing the cycle, it is currently unclear whether to include the thermal expansion term in predicting N_D using Eq. (3). This problem is due to a lack of understanding of the physical phenomena taking place during the cycle which is exacerbated by experimental uncertainty in the actual sample temperature which may differ from the bath temperatures.

Herklotz *et al.*[10] reported the phase diagram of [001]-poled PMN-28PT single crystals in the electric field vs. temperature (E-T) diagram under zero compressive stress. The phase boundaries were found to be dependent on both E and T.[10] PMN-28PT successively assumed the phases rhombohedral (R), monoclinic M_A, monoclinic M_C, tetragonal (T), and cubic (C) as temperature increased from 22 to 165 °C. The polarization vector was oriented in the (111), (110), (010), and (001) directions for the R, M_A, M_C, and T phases, respectively.[10,11] This corresponds to continuous rotation and increase in polarization with each phase transition from the R phase to the T phase.[12] Note that some samples did not transition into the M_C phase.[10] Furthermore, the ferroelectric-paraelectric phase transition under zero field occurred at $T_{Curie} = 126$ °C.[10] Above T_{Curie}, a pseudocubic (PC) phase (paraelectric) existed featuring local lattice distortions.[13] However, even at temperatures above T_{Curie}, an applied electric field can cause the growth of ferroelectric domains in the T phase from the paraelectric pseudocubic phase.[14] This phenomenon is apparent in the double hysteresis loops in the D-E diagram.[15] As the temperature increases above T_{Curie}, the paraelectric state becomes more and more stable and the electric field required to induce the ferroelectric state increases.[10] Zhou *et al.*[16] reported d_{33} and s_{33} at room temperature to be 2365 pC/N and 86.46 pm^2/N, respectively. Slodczyk[17] reported that the lattice parameter a_T of [001]-oriented PMN-28PT increased as the temperature increased from 0 to 110 °C under zero electric field. It decreased slightly around 110 °C and then increased further with temperature up to 320 °C.

This paper aims to elucidate the dynamic effects of thermal expansion and field induced phase transitions on the energy density generated during the Olsen cycle. It identifies the circumstances under which the contribution of the secondary pyroelectric effect is important.

Single crystal PMN-28PT samples were purchased from Sinoceramics LLC State College, PA, USA. The dimensions of the samples were $5 \times 5 \times 3\,mm^3$. The two $5 \times 5\,mm^2$ faces of the samples were entirely coated with Cr/Au electrodes. The samples were oriented and poled in the [001]-direction.

The Olsen cycle was performed using an experimental setup consisting of the electrical and thermal subsystems described in detail in Refs. 7 and 18. In brief, the thermal subsystem was composed of two isothermal silicone oil baths held at constant and uniform temperatures $T_C = 22$ °C and $T_H = 140$ °C. The electrical subsystem consisted of a high-voltage power amplifier and a Sawyer-Tower circuit.[19] Note that the sample temperature was not measured to avoid electrical conduction between the thermocouple and the sample. Alternatively, the lumped capacitance approximation[20] can be used to predict the sample temperature $T_s(t)$ after it is transferred from the hot silicone bath at $T_H = 140$ °C to the cold one at 22 °C during the Olsen cycle. It is valid when the Biot number, defined as $Bi = h(t)\,L/k$, is much smaller than 1.0, where $h(t)$ is the time-dependent heat transfer coefficient, L is the sample characteristic length, and k is its thermal conductivity. The energy conservation equation is given by $\rho c_p V dT_s/dt = -h(t)A_s(T_s - T_C)$, where A_s and V are the surface area and volume of the sample, i.e., $A_s = 1.1\,cm^2$ and $V = 0.075\,cm^3$. The heat transfer coefficient $h(t)$ due to natural convection was estimated based on a correlation given in Ref. 21 to find an analytical expression for $T_s(t)$ presented in supplementary material.[26]

First, isothermal bipolar D-E loops were collected by applying a triangular voltage signal at 0.1 Hz across the single crystal samples in silicone oil baths between 22 and 170 °C by increments of 10 °C. This corresponded to an electric field varying from −0.75 to 0.75 MV/m. The saturation polarization $P_s(T)$ and the large-field dielectric constant $\epsilon_r(T)$ were retrieved by fitting the linear portion of each D-E loop corresponding to electric field decreasing from 0.75 to 0.2 MV/m with Eq. (1) for each temperature. Then, the Olsen cycle was performed by consecutively dipping the samples in the hot and cold silicone oil baths while cycling the electric field between $E_L = 0.2\,MV/m$ and $E_H = 0.75\,MV/m$. The cycle was performed at two different cycle frequencies, namely, 0.0173 and 0.0211 Hz. The lowest cycle frequency allowed the electric displacement D to reach a steady state before the next process of the Olsen cycle was performed, corresponding to quasiequilibrium conditions. At higher frequency, isothermal processes 1-2 and 3-4 were performed after processes 4-1 and 2-3 as soon as the electric displacement reached a maximum or minimum, respectively.

Finally, in order to compare experimental results and predictions by Eq. (3), the thermal expansion coefficient α_3

was necessary. The latter can be estimated from the lattice parameter $a_T(T)$ according to[22]

$$\alpha_3(T) = \frac{1}{a_T}\frac{da_T}{dT}. \quad (4)$$

Here, $\alpha_3(T)$ for PMN-28PT was computed numerically using a third order polynomial spline fit of the experimental data reported by Slodczyk[17] between 7 and 200 °C. Then, the strain x_3 was computed by numerically integrating $\alpha_3(T)$ between T_C and T using the trapezoidal rule. The zero-field lattice parameter $a_T(T)$ (Ref. 17) and the corresponding thermal expansion coefficient $\alpha_3(T)$ as a function of temperature for PMN-28PT are presented in the supplemental material.[26]

Table I summarizes the properties of [001] PMN-28PT needed in the model given by Eq. (3). The piezoelectric coefficient d_{33} and the elastic compliance s_{33} at 22 °C were reported in the literature.[16] The strain x_3 was estimated between 22 and 90 °C as well as between 22 and 140 °C from the lattice parameter reported by Slodczyk,[17] as previously discussed. It should be noted that x_3 between 22 and 90 °C represents more than 70% of its value between 22 and 140 °C. In addition, $P_s(T)$ and $\epsilon_r(T)$ were retrieved from the D-E loops at 22, 90, and 140 °C based on Eq. (1).

Fig. 2 shows the isothermal bipolar D-E loops taken at 22, 90, and 140 °C. The D-E loops at 22 and 90 °C featured high remnant and saturation polarizations, indicating that the sample was in a ferroelectric state. Interestingly, the D-E loop at 90 °C saturated at a displacement approximately 20% larger than that at 22 °C. The D-E loop at 140 °C showed double hysteresis characterized by paraelectric behavior (in pseudocubic phase) at low electric field and ferroelectric behavior at high electric field, due to field-induced phase transition.

Fig. 2 also shows the Olsen cycles performed at 0.0173 and 0.0211 Hz for $T_C = 22$ °C and $T_H = 140$ °C while the electric fields were taken as $E_L = 0.2$ MV/m and $E_H = 0.75$ MV/m. The Olsen cycle was plotted in the D-E diagram by matching state 3 of the cycle with the D-E loop at 140 °C at electric field 0.75 MV/m, as performed by Olsen and Evans.[23] Indeed, only changes in displacement could be measured during the Olsen cycle and the isothermal bipolar D-E loop at T_{hot} typically overlaps well with that of process 3-4 in the Olsen cycle.[7,9] The two Olsen cycles shown in Figs. 2(a) and 2(b) were performed consecutively on the same PMN-28PT sample. It should be noted that the results were repeatable from one cycle to another and among PMN-28PT samples as observed with PZN-5.5PT.[8]

TABLE I. [001] PMN-28PT properties reported in the literature used in Eq. (3) to predict N_D.

Properties	Units				Ref.
T	(°C)	22	90	140	
P_s	(μC/cm^2)	19.11	23.05	16.78	
ϵ_r	…	3475	2037	4026	
d_{33}	(pC/N)	2365	…	…	16
s_{33}	(pm^2/N)	86.46	…	…	16
x_3 (from 22 °C to T)	(%)	…	0.0831	0.1154	

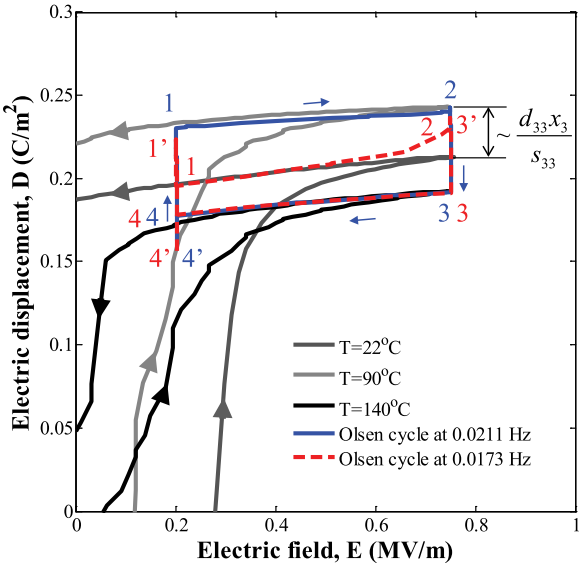

FIG. 2. Isothermal bipolar D-E loops at T = 22, 90, and 140 °C and experimental Olsen cycles at 0.0173 and 0.0211 Hz for PMN-28PT with $E_L = 0.2$ MV/m, $E_H = 0.75$ MV/m, $T_C = 22$ °C, and $T_H = 140$ °C.

The Olsen cycle performed at lower frequency followed the path of the isothermal D-E loops at 22 and 140 °C except during process 1-2 for electric fields between 0.65 and 0.75 MV/m. By contrast, the Olsen cycle performed at higher frequency extended beyond the electric displacement span of the isothermal D-E loops at 22 and 140 °C for the entire electric field span between E_L and E_H. This difference can be attributed to the fact that when process 1-2 was performed at higher frequency, the sample did not have time to reach the temperature of the cold oil bath during the cooling process 4-1, i.e., $T_{cold} > T_C$. In fact, the D-E loop at 90 °C was found to closely match the electric displacement of the Olsen cycle at 0.0211 Hz. Moreover, the Olsen cycle shown in Fig. 2(a) features spikes at points 1, 2, and 3′. A similar spike at point 2 was observed by Olsen and Bruno[24] with polyvinylidene fluoride. In addition, for both frequencies, points 4 and 4′ did not fall on the same point due to leakage current through the sample at high temperature and electric field.[18,24] The following sections explain the physical phenomena responsible for the spikes observed in the lower frequency Olsen cycle.

Fig. 3 shows the electric displacement measured as a function of time for Olsen cycles performed at 0.0173 and 0.0211 Hz. States 1 through 4′ correspond to those shown in Fig. 2. Note that, for both frequencies, processes 1-2 and 3-4 were performed in 1.5 s while the heating time τ_{23} was 27 s. Thus, changes in the sample temperature during processes 1-2 and 3-4 were negligible compared with those in processes 2-3 and 4-1. For the lower frequency, the cooling time τ_{41} was identical to the heating time τ_{23}, i.e., $\tau_{41} = \tau_{23} = 27$ s. However, it was shorter ($\sim$17 s) for the higher frequency cycle. Thus, the sample temperature reached the hot bath temperature $T_H = 140$ °C for both frequencies but did not have time to reach the cold bath temperature $T_C = 22$ °C for higher frequency. In the Olsen cycle performed at 0.0211 Hz, the electric displacement reached a maximum during the cooling process 4-1 immediately before performing the isothermal charging process 1-2. In this case, the duration of the cooling process 4-1 was 17 s. However, for the cycle performed at

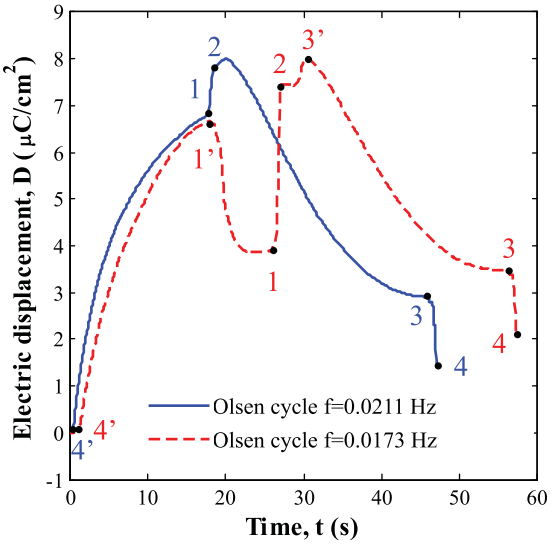

FIG. 3. Measured electric displacement vs. time during the Olsen cycles at 0.0211 and 0.0173 Hz, respectively. Here, $T_C = 22\,^{\circ}\text{C}$, $T_H = 140\,^{\circ}C$, $E_L = 0.2\,\text{MV/m}$, and $E_H = 0.75\,\text{MV/m}$.

0.0173 Hz, the sample was held in the cold bath at 22 °C for an additional 10 s for a total of 27 s before performing process 1-2. During this additional time, the material cooled down and de-poled as a result of a phase transition, and the electric displacement reached a steady state around 4 $\mu\text{C/cm}^2$.

Fig. 4 plots the Olsen cycles, performed in this study, in the E-T phase diagram of [001]-oriented PMN-28PT reported by Herklotz *et al.*[10] It also shows the crystalline structure of each phase and the corresponding polarization. The shaded region corresponds to conditions when the material has been electrically induced into a ferroelectric state but possesses electric displacements smaller than those of the T phase as discussed by Merz.[15] The E-T phase diagram suggests that during the cooling process 4-1 of the Olsen cycle at higher frequency of 0.0211 Hz, the material transitioned from a pseudocubic state at $T_{hot} = T_H = 140\,^{\circ}\text{C}$ to the highly polarized T phase at $T_{cold} = 90\,^{\circ}\text{C}$ where it remained at state 1 (on blue cycle). Indeed, the sample did not have time to reach the cold bath temperature of $T_C = 22\,^{\circ}\text{C}$. Instead, it reached about 90 °C, as suggested by the superposition of the D-E loop at 90 °C and process 1-2 of the Olsen cycle shown in Fig. 2. This was corroborated by predictions from the lumped capacitance approximation presented in the supplementary material.[26] Thus, the sample retained the polarization generated by the pseudocubic to T phase transition at state 1. On the other hand, at lower cycle frequency of 0.0173 Hz, the polarization that appeared from the pseudocubic to T phase transition (state 1′) disappeared during further cooling down to $T_{cold} = T_C = 22\,^{\circ}\text{C}$ as the sample underwent subsequent phase transitions to the less polarized monoclinic phases[10] where it remained at state 1.

Furthermore, at lower frequency, we speculate that the sample underwent a phase transition from M_A to M_C phase during process 1-2 of the cycle. Then, the deviation of the Olsen cycle from the D-E loop at 22 °C near state 2 (Fig. 2) can be attributed to electric-field-induced phase transition from M_A to M_C phase. Indeed, the M_C phase is more polarized than the M_A phase due to the continuous polarization rotation occurring between the R and T phases.[12] Finally, the

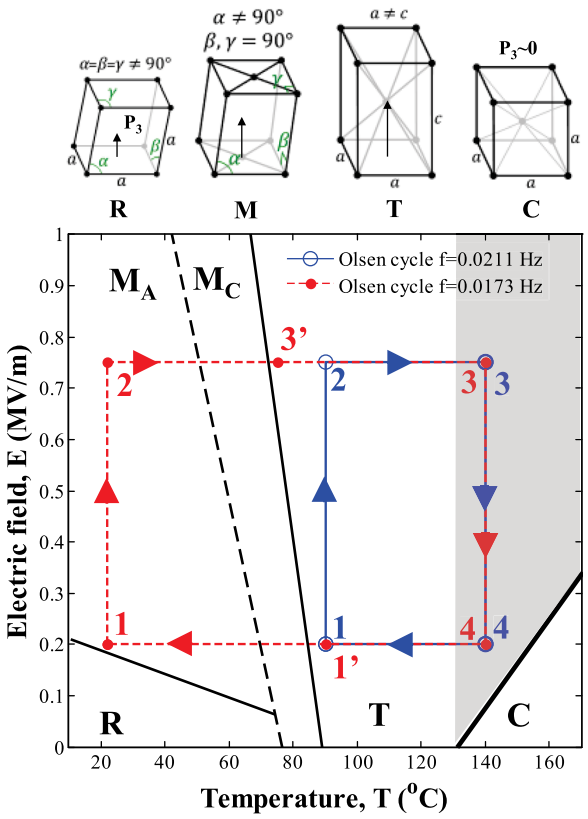

FIG. 4. Olsen cycles performed at 0.0173 and 0.0211 Hz in the E-T diagram and phase boundaries for [001]-poled PMN-28PT (Ref. 11). The $M_A - M_C$ phase boundary (dashed lines) was not always observed. The shaded region corresponds to electrically induced ferroelectric state with polarizations smaller than that of the T phase (Ref. 16).

spike between states 2 and 3′ can be attributed to the sample transitioning from the M_C phase to the T phase during the heating process 2-3 before transitioning to the pseudocubic phase at state 3 (Fig. 4).

The energy density measured experimentally for the lower frequency Olsen cycle at 0.0173 Hz was 12.5 J/l. That predicted by Eq. (3) using properties at $T_C = 22\,^{\circ}\text{C}$ and $T_H = 140\,^{\circ}\text{C}$ reported in Table I and ignoring the thermal expansion term was 11.5 J/l. For the higher frequency Olsen cycle at 0.0211 Hz, the measured energy density was 27.6 J/l. Equation (3) predicted an energy density of 28.9 J/l using properties at $T_C = 22\,^{\circ}\text{C}$ and $T_H = 140\,^{\circ}\text{C}$ and accounting for thermal expansion between 22 and 140 °C. The model predictions fell within 8.0% and 5.0% of the energy densities measured experimentally for the cycles at lower and higher frequency, respectively. This good agreement indicates that the additional energy density obtained at higher frequency can be attributed to the secondary pyroelectric effect accounted for by the thermal expansion term $d_{33}x_3/s_{33}$ estimated to be $0.033\,\text{C/m}^2$. In addition, Fig. 2 suggests that the displacement in the D-E loop at 90 °C between states 1 and 2 is equal to that for 22 °C translated by a displacement $d_{33}x_3/s_{33}$ or $P_s(90\,^{\circ}\text{C}) = P_s(22\,^{\circ}\text{C}) + d_{33}x_3/s_{33}$ (see Fig. 2). In fact, the difference between the upper portion of the D-E loops at 90 °C and 22 °C for electric field decreasing from E_H to E_L was $0.034 \pm 0.003\,\text{C/m}^2$ and fell within 2.9% of the estimated value of $d_{33}x_3/s_{33}$. Consequently, using the properties $\epsilon_r(T)$ and $P_s(T)$ in Table I between $T_{cold} = 90\,^{\circ}\text{C}$

and $T_{hot} = 140\,^{\circ}\mathrm{C}$ and ignoring thermal expansion in Eq. (3) predicted an energy density of 29.9 J/l which fell within 8.4% of that measured experimentally at 0.0211 Hz. These results demonstrate that the D-E loops at the actual sample temperatures include the contribution of the secondary pyroelectric effect. Thus, if the actual sample temperature is known, the thermal expansion term in Eq. (3) should be ignored in predicting the energy density.

All pyroelectric materials are also piezoelectric and a positive thermal expansion corresponds to a positive change in polarization within the material as described by the secondary pyroelectric coefficient. Thus, performing the Olsen cycle on PMN-28PT between the T and pseudocubic phases, when the thermal expansion is entirely positive during cooling, resulted in larger energy density than when cooling from the pseudocubic to the monoclinic phase region, when negative thermal expansion occurs. Thus, higher energy density was achieved at higher cycle frequency by limiting the temperature swing and the phase transition from the T to the pseudocubic phase. In addition, the combination of larger energy density and higher cycle frequency resulted in larger power density. Performing the Olsen cycle at higher frequency also reduced the thermal stress on the samples which could increase their lifetime.

This interpretation was also valid for results reported for PMN-32PT,[7] PZN-5.5PT,[8] and 8/65/35 PLZT.[9] Indeed, Kandilian *et al.*[7] performed the Olsen cycle on [001]-oriented PMN-32PT with cold source temperature $T_C = 80\,^{\circ}\mathrm{C}$ and $E_L = 0.2\,\mathrm{MV/m}$. These conditions were near the phase boundary between T and M_C phases of PMN-32PT estimated to be at 0.2 MV/m and 85 °C.[25] At 80 °C, the material was likely in the M_C phase featuring a polarization smaller than that of the T phase. However, for the cycle frequency considered, the samples' temperature did not fall below 85 °C during the Olsen cycle. In fact, Kandilian *et al.*[7] performed process 1-2 as soon as the electric displacement had reached a maximum. This was identical to the way the Olsen cycle at 0.021 Hz was performed. Thus, the samples did not undergo the T to M_C phase transition. Then, the presence of the T phase and the associated large polarization caused electric displacement span in the Olsen cycle to extend beyond that of the isothermal bipolar D-E loop at 80 °C.[7] Finally, the energy density of the Olsen cycle could be predicted by accounting for the secondary pyroelectric coefficient in Eq. (3) using $T_C = 80\,^{\circ}\mathrm{C}$ and $T_H = 130$ and $140\,^{\circ}\mathrm{C}$.[7]

The Olsen cycle performed on PZN-5.5PT was characterized by sample temperature larger than 100 °C (Ref. 8) corresponding to the T phase for all electric fields considered according to the PZN-4.5PT phase diagram.[11] Similarly, for Olsen cycles performed on 8/65/35 PLZT ceramics with T_C equal to 45 and 65 °C,[9] the samples remained in the ferroelectric phase away from any phase boundaries.[9] Thus, in the absence of phase boundaries near T_C and E_L, thermal expansion did not contribute significantly to energy generation and could be ignored in the physical model given by Eq. (3). This resulted in good predictions of the experimental data.[8,9]

Overall, in order to maximize the energy density of the Olsen cycle while maintaining a large power density, E_L and T_{cold} should be chosen so that the material exhibits the highest electric displacement. This is not necessarily achieved by maximizing $(T_{hot} - T_{cold})$. Instead, the material should undergo a single phase transition resulting in the highest change in polarization. In the case of PMN-28PT and PMN-32PT, this corresponds to the transition from the pseudocubic to the tetragonal phase.

This research was supported in part by NSF-IGERT program Clean Energy for Green Industry at UCLA (NSF Award 0903720).

[1]R. B. Olsen, D. A. Bruno, J. M. Briscoe, and W. F. Butler, Ferroelectrics **38**, 975 (1981).
[2]S. B. Lang, *Sourcebook of Pyroelectricity* (Gordon and Breach, New York, NY, 1974).
[3]S. B. Lang and D. K. Das-Gupta, *Handbook of Advanced Electronic and Photonic Materials and Devices* (Academic, San Diego, CA, 2001), Vol. 4.
[4]M. E. Lines and A. M. Glass, *Principles and Applications of Ferroelectrics and Related Materials* (Clarendon, Oxford, UK, 1977).
[5]Z. Li, Z. Xi, Z. Xu, and X. Yao, J. Mater. Sci. Lett. **21**, 1325 (2002).
[6]M. W. Hooker, *Properties of PZT-Based Piezoelectric Ceramics Between −150 and 250 °C* (Citeseer, 1998).
[7]R. Kandilian, A. Navid, and L. Pilon, Smart Mater. Struct. **20**, 055020 (2011).
[8]I. M. McKinley, R. Kandilian, and L. Pilon, Smart Mater. Struct. **21**, 035015 (2012).
[9]F. Y. Lee, S. Goljahi, I. M. McKinley, C. S. Lynch, and L. Pilon, Smart Mater. Struct. **21**, 025021 (2012).
[10]A. Herklotz, J. D. Plumhof, A. Rastelli, O. G. Schmidt, L. Schultz, and K. Dorr, J. Appl. Phys. **108**, 094101 (2010).
[11]A.-E. Renault, H. Dammak, G. Calvarin, and P. Gaucher, J. Appl. Phys. **97**, 044105 (2005).
[12]V. H. Schmidt, R. Chien, I.-C. Shih, and C.-S. Tu, AIP Conf. Proc. **677**, 160–167 (2003).
[13]J. Han and W. Cao, Phys. Rev. B **68**, 134102 (2003).
[14]N. Srivastava and G. J. Weng, J. Appl. Phys. **99**, 054103 (2006).
[15]W. J. Merz, Phys. Rev. **91**, 513 (1953).
[16]D. Zhou, F. Wang, L. Luo, J. Chen, W. Ge, X. Zhao, and H. Luo, J. Phys. D: Appl. Phys. **41**, 185402 (2008).
[17]A. Slodczyk, "Structural, dielectric and vibrational studies of lead magnesium niobate-lead titanate $(1\text{-}x)PbMg_{1/3}Nb_{2/3}O_3\text{-}xPbTiO_3$ solid solutions," Ph.D. dissertation (University of Silesia, 2006).
[18]A. Navid and L. Pilon, Smart Mater. Struct. **20**, 025012 (2011).
[19]C. B. Sawyer and C. H. Tower, Phys. Rev. **35**, 269 (1930).
[20]F. P. Incropera, D. P. DeWitt, T. Bergman, and A. Lavine, *Fundamentals of Heat and Mass Transfer*, 6th ed. (John Wiley and Sons, Ltd., New York, NY, 2006).
[21]E. M. Sparrow and A. J. Stretton, Int. J. Heat Mass Transfer **28**, 741 (1985).
[22]G. Bhikshamaiah, S. Annapurna, and A. K. Singh, Cryst. Res. Technol. **41**, 911 (2006).
[23]R. B. Olsen and D. Evans, J. Appl. Phys. **54**, 5941 (1983).
[24]R. B. Olsen and D. A. Bruno, in *Proceedings of the 21st Intersociety Energy Conversion Engineering Conference, American Chemical Society* (San Diego, CA, 1986), pp. 89–93.
[25]L. S. Kamzina and H. Luo, Phys. Solid State **51**, 2316 (2009).
[26]See supplementary material at http://dx.doi.org/10.1063/1.4776668 for thermal properties of PMN-28PT and thermal analysis of cooling process 1-4.